Absent pinch points and emergent clusters: Further neighbor interactions in the pyrochlore Heisenberg antiferromagnet

P. H. Conlon* and J. T. Chalker
Theoretical Physics, Oxford University, 1 Keble Road, Oxford OX1 3NP, United Kingdom
(Received 1 April 2010; revised manuscript received 14 May 2010; published 7 June 2010)

We discuss the origin of spin correlations observed in neutron-scattering experiments on the paramagnetic phase of a number of frustrated spinel compounds, most notably $ZnCr_2O_4$. These correlations are striking for two reasons. First, they have been interpreted as evidence for the formation of weakly interacting hexagonal clusters of spins. Second, they are very different from those calculated for the nearest-neighbor Heisenberg pyrochlore antiferromagnet, in which Coulomb-phase correlations generate sharp scattering features known as pinch points. Using large-n calculations and Monte Carlo simulations, we show that very weak further neighbor exchange interactions can account for both the apparent formation of clusters and the suppression of pinch points.

DOI: 10.1103/PhysRevB.81.224413 PACS number(s): 75.10.Hk, 75.50.Ee, 61.05.fd

I. INTRODUCTION

A central reason for interest in geometrically frustrated magnets is that they are systems which can support strong correlations without developing long-range order. This cooperative paramagnetic behavior appears at temperatures small compared to the main interaction scale, which is characterized by the magnitude of the Curie-Weiss constant Θ_{CW}. The absence of long-range order at low temperature can be understood in the framework of classical models with nearest-neighbor (NN) interactions, as a consequence of macroscopic ground-state degeneracy.[1]

Results from recent neutron-scattering studies of some important examples of geometrically frustrated magnets present a paradox, and our aim in this paper is to offer a resolution of the paradox. More specifically, experiments on a number of spinel compounds, including, in particular, $ZnCr_2O_4$, have been interpreted as revealing the formation of small, independent clusters of spins.[2–5] In contrast, the minimal theoretical model which is assumed to describe these systems, the nearest-neighbor Heisenberg pyrochlore antiferromagnet, is notable for a quite different feature: pinch-point scattering, indicative of algebraic correlations. We show in this paper that further neighbor (FN) interactions strongly influence scattering in the cooperative paramagnetic phase. Very weak further neighbor interactions of the appropriate sign (ferromagnetic second neighbor or antiferromagnetic third neighbor) are sufficient to suppress pinch-point scattering and generate quite accurately the short-range correlations that have been interpreted in terms of independent spin clusters.

The spinel compounds, AB_2O_4, have a structure in which the B sites form a three-dimensional network of corner-sharing tetrahedra known as a pyrochlore lattice (Fig. 1). The same lattice is realized by both A and B sites in the pyrochlore compounds $A_2B_2O_7$ and in the Laves phase compounds with formula AB_2. Evidence for spin clusters has been reported in the chromites, ACr_2O_4 with nonmagnetic A=Zn, Mg, and Cd as well as in the ferrite $CdFe_2O_4$ (Refs. 2–5, respectively). In all cases, the strong similarity between experimentally measured spin correlations and the form factor for independent hexagonal clusters leads to an interpretation in terms of independent spin clusters. Results for $Y(Sc)Mn_2$ have broadly similar features.[6] Clusterlike correlations are also observed in the spin ice compound $Dy_2Ti_2O_7$: here it has been argued from comparison with simulations that they arise from further neighbor interactions.[7] Spin clusters are not universally observed in frustrated pyrochlore magnets, however. Among the spin ice compounds, compelling evidence for pinch-point scattering is seen in $Ho_2Ti_2O_7$.[8] For a recent review of properties of the frustrated spinels, see Ref. 9.

The classical nearest-neighbor antiferromagnetic Heisenberg model on this lattice (which we refer to as the NN *model*) is now well understood theoretically.[10–12] The model has no phase transition and remains in the paramagnetic phase down to temperature T=0. The low-temperature re-

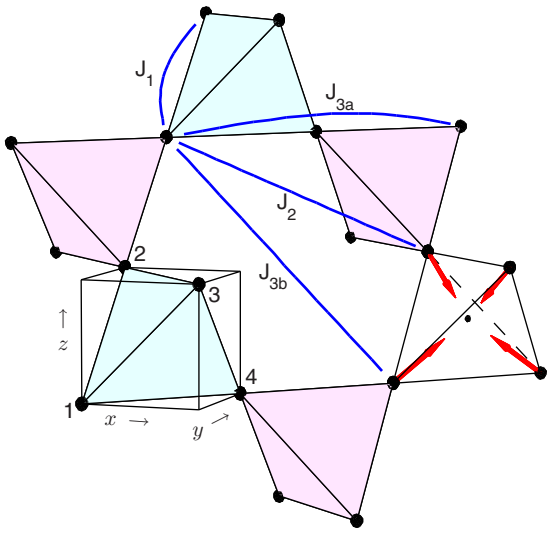

FIG. 1. (Color online) Pyrochlore lattice, illustrating the first-, second-, and third-neighbor couplings. There are two inequivalent third-neighbor interactions, but for J_{3a}=J_{3b}, we use J_3 to denote both. Numbers indicate sublattice labeling. The centers of the tetrahedra form a diamond lattice and the arrows show the choice made to orient the diamond-lattice bonds.

gime is nevertheless strongly correlated. The nearest-neighbor interaction energy is minimized by any spin configuration for which the magnetization on every tetrahedron vanishes, giving a ground-state manifold with a macroscopic number of degrees of freedom. While states on this manifold are weighted differently by thermal fluctuations, order-by-disorder effects are too weak to induce a Néel state. Simulations of neutron scattering show sharp features in the structure factor.[13] Known as pinch points, a clear understanding of their origin comes from the recognition that ground states of the NN model can be mapped onto configurations of a solenoidal lattice vector-field[14,15] (this mapping will be reviewed in Sec. II B) whose long-wavelength fluctuations are governed by an entropic Maxwell action. The pinch points in scattering are a consequence of dipolar correlations of the solenoidal field. (For a recent review of models with such a Coulomb phase, see Ref. 16.) Although algebraic at $T=0$, at finite temperature spin correlations decay exponentially beyond a correlation length $\xi_{\|}$ and pinch points acquire a width $\sim\xi_{\|}^{-1}$. For spin ice, the correlation length diverges exponentially as $T\to 0$ due to the finite energy cost for violations of the ice rules, but for the NN model with continuous degrees of freedom, only as $T^{-1/2}$. Since the NN model unambiguously gives rise to pinch points in scattering when $T \ll \theta_{\mathrm{CW}}$, with thermal broadening at finite temperature, their absence in experiments on the paramagnetic phase of the frustrated spinels demands an explanation which goes beyond the NN model.

Here we extend the NN model by including further neighbor exchange terms (see Fig. 1 for definitions) and consider their effect on paramagnetic scattering. Further neighbor terms, both ferromagnetic (FM) and antiferromagnetic (AFM), will, in general, have two effects: (i) to change scattering in the paramagnetic phase; (ii) to induce ordering at a low T. With regard to ordering transitions out of the low-temperature paramagnetic phase, the role of further neighbor exchange has been considered before: from a mean-field perspective, Reimers *et al.*[17] examined possible ordered states with further neighbor exchange; and following simulations by Tsuneishi *et al.*,[18] a detailed study by Chern *et al.*[19] of the phase diagram with a weak J_2 confirmed the mean-field predictions. There has been less work to pin down the effect of further neighbor exchange on paramagnetic scattering in Heisenberg models, although we note that an analysis of neutron-scattering data using third neighbors has been done for the frustrated spinel $ZnFe_2O_4$, which has ferromagnetic nearest-neighbor interactions.[20] In spin ice, Yavors'kii *et al.*[7] have shown with extensive simulations that further neighbor interactions can promote clusterlike scattering.

Our main results are as follows: first, further neighbor exchange terms of the right sign (FM J_2 or AFM J_3) can be effective both at suppressing pinch-point scattering intensity and at broadening pinch points; and second, within the manifold of NN ground states, they favor states with clusterlike correlations. These effects are noticeable even at temperatures two orders of magnitude larger than the temperature of the transition that the additional interactions induce. Using the language of the Coulomb-phase description, these effects are summarized in part by the fact that further neighbor terms renormalize the Coulomb-phase coupling constant.

A visual impression of our findings in relation to experimental reports of spin clusters is given by comparing figures that show the computed diffuse scattering in two cases. The first case is the nearest-neighbor model, for which pinch points, broadened by finite temperature, are apparent in Figs. 3(a) and 3(b). The second case is a model with additional weak further neighbor interactions, for which behavior is shown in Figs. 3(c) and 3(d). In this case scattering at the positions of pinch points is heavily suppressed. In its place, rings of scattering intensity are formed of the kind that have been interpreted as indications of spin cluster formation in Refs. 2–5.

The remainder of this paper is organized as follows. In Sec. II we present the model and detail the main analytic tool used, a self-consistent Gaussian approximation which is exact for n-component spins in the large-n limit. Here we also review the mapping to lattice vector-fields, which facilitates a more straightforward discussion of the long-wavelength physics in the vicinity of pinch points. In Sec. III we consider the effect of a FM J_2 or an AFM J_3 which are of the sign required to induce clusterlike scattering and suppress pinch points. In Sec. IV, we summarize the effects of AFM J_2 or FM J_3, and we look briefly at other combinations in Sec. V. In Sec. VI we discuss dynamics, describing how we expect the effects of further neighbor interactions to be more conspicuous in quasielastic scattering than in static correlations. We consider estimates of further neighbor exchange for relevant compounds in Sec. VII. We summarize our results in Sec. VIII. Further details of various calculations can be found in Ref. 21.

II. MODEL AND THEORETICAL APPROACH

Our focus is on the low-temperature behavior in the paramagnetic phase of the classical isotropic Heisenberg model with Hamiltonian

$$H = \frac{1}{2}\sum_{ij} J_{ij}\mathbf{S}_i \cdot \mathbf{S}_j, \tag{1}$$

where the degrees of freedom are unit length, three-component vectors residing on the sites of the pyrochlore lattice and where the dominant interaction is nearest-neighbor antiferromagnetic (see Fig. 1). It is known that behavior of the nearest-neighbor Heisenberg model is very well approximated by the large-n limit of its generalization to n-component spins.[14,22]

We also use this large-n limit. Through its equivalence to a spherical model,[23] we present our method in the language of a self-consistent Gaussian approximation (SCGA). The validity of this approach is confirmed by the excellent agreement with Monte Carlo (MC) simulations on the Heisenberg model, Eq. (1), both with and without further neighbor terms—results from Monte Carlo simulations appear as points in figures and results from the following analysis as solid lines. Our simulations were performed using the

Metropolis algorithm for systems of 2048 spins and 16 384 spins. The longest runs, required for the lowest temperatures, were 10^8 MC steps per spin. In general though, run lengths were chosen in order that the statistical errors are smaller than the symbol size in the plots.

A. Self-consistent Gaussian approximation

We replace fixed length spins $\mathbf{S}_i$ with soft ones, denoting the magnitude of one component by s_i. Soft spin configurations are weighted by $e^{-\beta\mathcal{H}}$, where

$$\beta\mathcal{H} = \frac{1}{2}\sum_{ij}\left(\lambda\delta_{ij} + \beta\sum_n J_n V_{ij}^{(n)}\right)s_i s_j. \tag{2}$$

The value of the Lagrange multiplier λ is chosen to ensure $\langle s_i^2\rangle = 1/3$ as required for a single component of a unit length three-component vector in a paramagnetic phase. The mth-neighbor interaction matrices $V_{ij}^{(m)}$ are related to the respective adjacency matrices by addition of multiples of the identity in the way described in Appendix B and these (seemingly arbitrary) choices of the diagonal entries are dictated by our subsequent interpretation of λ as the stiffness of a Coulomb-phase action. The multiplier λ is determined self-consistently by the condition on the average spin length

$$\frac{1}{3} = \frac{1}{4N}\mathrm{Tr}\left[\lambda I + \beta\sum_n J_n V^{(n)}\right]^{-1},$$

where $4N$ is the total number of sites. The translational symmetry of the system ensures that the interactions are block diagonal in reciprocal space (see Appendix A for Fourier transform conventions), and the self-consistency condition can be written in that basis as

$$\frac{1}{3} = \frac{1}{4N}\sum_{\mathbf{q}\in \mathrm{BZ}}\mathrm{Tr}\left[\lambda I + \beta\sum_n J_n V^{(n)}(\mathbf{q})\right]^{-1}, \tag{3}$$

where the matrices $V^{(n)}(\mathbf{q})$ act within the space of the four sublattices. Their explicit forms are provided in Appendix B. The solutions for λ for various choices of further neighbor exchange are shown in Fig. 2. We discuss analytical bounds on the solution following Eq. (10), after the physical significance of λ as the stiffness of a Coulomb-phase action has been made clear.

The correlation functions in reciprocal space between different sublattices are

$$\langle s_\mu(\mathbf{q}) s_\nu^*(\mathbf{q})\rangle = \left[\lambda I + \beta\sum_n J_n V^{(n)}(\mathbf{q})\right]^{-1}_{\mu\nu} \tag{4}$$

and the static structure factor is the sum of all 16 such correlators. For the nearest-neighbor model this can be obtained analytically at all temperatures in a palatable form: at $T=0$, it is provided by Isakov *et al.*[14] (with a different sublattice labeling convention) and for completeness we provide the full, finite temperature form in Eq. (D1) in Appendix D. In the general case where further neighbor terms are not all zero and analytic expressions are unilluminating, spin correlations at any temperature can be straightforwardly obtained numerically from Eq. (4).

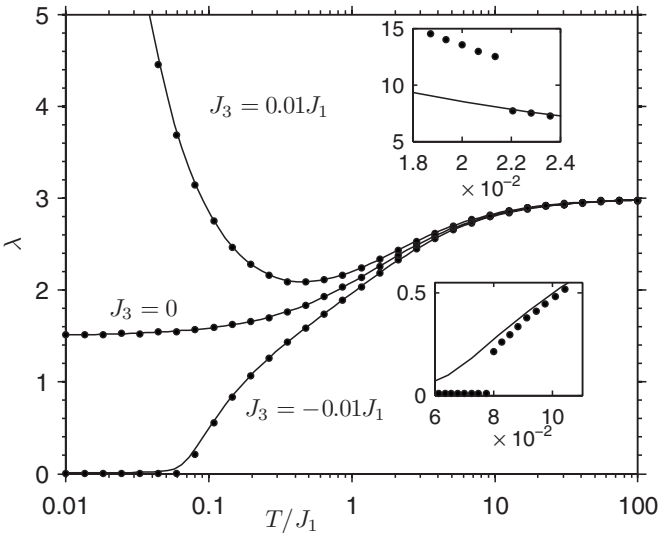

FIG. 2. Dependence of flux stiffness λ on temperature, showing influence of weak further neighbor interactions. Solid lines: solutions of Eq. (3) for the cases $J_3 = \pm 0.01J_1$ and $J_3 = 0$, all with $J_2 = 0$. Points: results from simulations on 2048 spins interpreted via Eq. (7). The effects of third-neighbor interactions are clearly noticeable even at temperatures two orders of magnitude larger than J_3. Insets: detailed behavior at low temperature; axes as in main panel. First-order phase transitions occur in simulations for both signs of J_3.

B. Mapping to long-wavelength description

Within the SCGA, Eqs. (3) and (4) give a full description of spin correlations in the paramagnetic phase. A more physical understanding comes from studying the long-wavelength physics in a way that allows comparisons with related models, including spin ice, interacting dimer models, and more generally any system with a Coulomb phase, such as those discussed in Ref. 16 and references therein.

In our context, the long-wavelength degrees of freedom emerge naturally after interpreting spin configurations as configurations of a lattice vector-field defined on the bonds of the diamond lattice. The mapping[14,15] is constructed as follows. Each site on a pyrochlore lattice is associated with a diamond bond, whose midpoint it is; the diamond lattice is bipartite so its bonds are orientable in a consistent way across the lattice. Therefore each spin component can be interpreted as the local magnitude of a lattice vector-field directed along diamond bonds. The merit of this description is that the vector field obtained is divergenceless in the limit $\beta J_1 \to \infty$ at fixed $\beta J_{n>1}$.

More precisely, for each spin component, labeled by α, define the flux field $\mathbf{B}^\alpha$ by $\mathbf{B}^\alpha(\mathbf{r}) = S^\alpha(\mathbf{r})\mathbf{e}(\mathbf{r})$, where $\mathbf{e}(\mathbf{r})$ is a (real-space) vector oriented along the diamond bond passing through the pyrochlore lattice site $\mathbf{r}$. The mapping has a straightforward implementation as a change in basis in reciprocal space

$$\begin{pmatrix} M^\alpha(\mathbf{q}) \\ B_x^\alpha(\mathbf{q}) \\ B_y^\alpha(\mathbf{q}) \\ B_z^\alpha(\mathbf{q}) \end{pmatrix} = \frac{1}{2}\begin{pmatrix} 1 & 1 & 1 & 1 \\ 1 & 1 & -1 & -1 \\ 1 & -1 & 1 & -1 \\ 1 & -1 & -1 & 1 \end{pmatrix}\begin{pmatrix} S_1^\alpha(\mathbf{q}) \\ S_2^\alpha(\mathbf{q}) \\ S_3^\alpha(\mathbf{q}) \\ S_4^\alpha(\mathbf{q}) \end{pmatrix}. \quad (5)$$

The directions of the vectors $\mathbf{e}(\mathbf{r})$ and the sublattice labeling are shown in Fig. 1. The vectors $\mathbf{e}(\mathbf{r})$ are taken to have length $\sqrt{3/4}$ (in contrast to the convention of unit length by Isakov *et al.*[14]) so that the definition of the mapping is consistent with the orthogonal change in basis in Eq. (5). At $\mathbf{q}=0$, the three spatial components of $\mathbf{B}$ are the three staggered magnetization order parameters which would describe a transition to $\mathbf{q}=0$ Néel order as referred to in Refs. 19 and 24. The experimentally accessible quantity is the structure factor which we define as $S(\mathbf{q})=4\langle|M(\mathbf{q})|^2\rangle$.

We are interested in the small-$\mathbf{q}$ behavior of the vector field $\mathbf{B}(\mathbf{q})$ but the experimental probe is via the linear combination $M(\mathbf{q})$. Consequently, the long-wavelength physics does not appear near $\mathbf{q}=0$ in the structure factor, but rather near $\mathbf{q}=\mathbf{K}$ for special vectors $\mathbf{K}$, which satisfy $M(\mathbf{q}+\mathbf{K}) \propto B_i(\mathbf{q})$ for some spatial direction i. The $\mathbf{K}$ are a subset of the reciprocal lattice vectors (see Appendix C).

Using this mapping, we now turn to the long-wavelength physics of the model defined in Sec. II A. We consider explicitly the case of $J_{3a}=J_{3b}\equiv J_3$ with all other further neighbor interactions zero; it is straightforward to carry out a similar analysis with any other choice of further neighbor terms.

At small $\mathbf{q}$ and $\beta J_1 \gg 1$, the linear combination $M(\mathbf{q})$ is nearly frozen out and within the SCGA we can legitimately read off a small-$\mathbf{q}$ theory for the field $\mathbf{B}$ by restricting the interaction to the 3×3 subblock which acts between the components of $\mathbf{B}$, providing λ is still calculated correctly using the full theory, Eq. (3). Further details are provided in Appendix B. By expanding the interactions to second order in $\mathbf{q}$ we obtain as a long-wavelength theory

$$\beta\mathcal{H} = \frac{1}{2}\sum_{\mathbf{q}} \lambda|\mathbf{B}(\mathbf{q})|^2 + \beta J_1 a^2|\mathbf{q}\cdot\mathbf{B}(\mathbf{q})|^2 - 8\beta J_3 a^2 q^2|\mathbf{B}(\mathbf{q})|^2. \quad (6)$$

The length scale a is the nearest-neighbor distance on the pyrochlore lattice. It is clear from Eq. (6) that J_1 acts purely to enforce the constraint $\mathbf{q}\cdot\mathbf{B}=0$.

We now consider the flux correlations that follow from Eq. (6). The $q=0$ flux fluctuations are straightforwardly obtained as

$$\langle B_i(\mathbf{q})B_j^*(\mathbf{q})\rangle_{\mathbf{q}=0} = \frac{1}{\lambda}\delta_{ij} \quad (7)$$

from which we identify the parameter λ as the dimensionless stiffness of the flux fields in the long-wavelength description. Since its original role as a Lagrange multiplier is to imitate the restrictions on phase space due to the fixed spin length, it is natural that it appears also as the stiffness which is entropic in origin. The correlation function in Eq. (7) is directly accessible from simulations and the data points in Fig. 2 follow from this relation; the same relation is used to measure the stiffness in simulations of dimer models [see, e.g., Eq. (2) in Ref. 25]. It is impressive that the SCGA captures behavior in the Heisenberg model so accurately.

The correlator for longitudinal flux fluctuations is

$$\langle B_x(q_x)B_x^*(q_x)\rangle_{q_y=q_z=0} = \frac{1}{\lambda}\left[\frac{\xi_\parallel^{-2}}{\xi_\parallel^{-2}+q_x^2}\right], \quad (8)$$

where we introduce the longitudinal correlation length $\xi_\parallel = a\sqrt{\beta(J_1-8J_3)/\lambda}$ (whose explicit form of course depends on which further neighbor exchanges are included). The inverse correlation length is the width of pinch points in reciprocal space. In the limit $\beta J_1 \to \infty$ at fixed βJ_3, flux fields are strictly solenoidal and $\xi_\parallel$ diverges. More generally, we emphasize that $\xi_\parallel$ depends on β both explicitly and through the β dependence of λ, via Eq. (3).

The transverse-flux correlations are

$$\langle B_z(q_x)B_z^*(q_x)\rangle_{q_y=q_z=0} = \frac{1}{\lambda}\left[\frac{1}{1-\frac{8\beta J_3 a^2}{\lambda}q_x^2}\right]. \quad (9)$$

For J_3 negative, the length $\xi_\perp = a\sqrt{8\beta|J_3|/\lambda}$ is the transverse correlation length for flux fluctuations. For positive J_3, $\xi_\perp$ is not a correlation length: instead it sets a length scale at which higher order terms in q must be included in the long-wavelength theory.

Youngblood and Axe[26] considered a phenomenological Landau free energy for polarization fluctuations in ferroelectrics, essentially identical to Eq. (6). Our discussion differs in that Eq. (6) is derived directly from a microscopic model, the parameter λ is allowed to flow, and moreover both positive and negative coupling to transverse gradient terms are considered.

Having established that λ has a physical interpretation as the Coulomb-phase coupling constant, we now turn to bounds on the value of λ which solves Eq. (3). Let $\varepsilon_{\min}$ be the minimum eigenvalue of $\Sigma_n J_n V^{(n)}(\mathbf{q})$ over all $\mathbf{q}$. The requirement that the quadratic form in Eq. (2) is positive-definite demands that $\lambda+\beta\varepsilon_{\min}>0$. Consequently we have

$$\lambda > -\beta\varepsilon_{\min}. \quad (10)$$

Taking an AFM J_1, we consider two special cases. First, for an AFM J_3 and all other $J_{n>1}=0$, we have $\varepsilon_{\min}=-16J_3$. Second, for a FM J_2 and all other $J_{n>1}=0$, the position of the minimum in reciprocal space is given by Chern *et al.*[19] in their Eq. (4) with $\varepsilon_{\min}\simeq -8.57|J_2|$ for $|J_2|\ll J_1$.

III. CONSEQUENCES OF AFM J_3 OR FM J_2

A. Paramagnetic phase

Within the paramagnetic phase, AFM J_3 or FM J_2 act to suppress pinch points and to promote clusterlike correlations. These effects are shown in Fig. 3, which should be compared, for example, with Fig. 3 of Ref. 2. The behavior illustrated here is one of our main results. Its origin is discussed in this section.

1. Consequences for pinch-point visibility

The pinch points are the signature of algebraic correlations in a Coulomb phase. There are three ways in

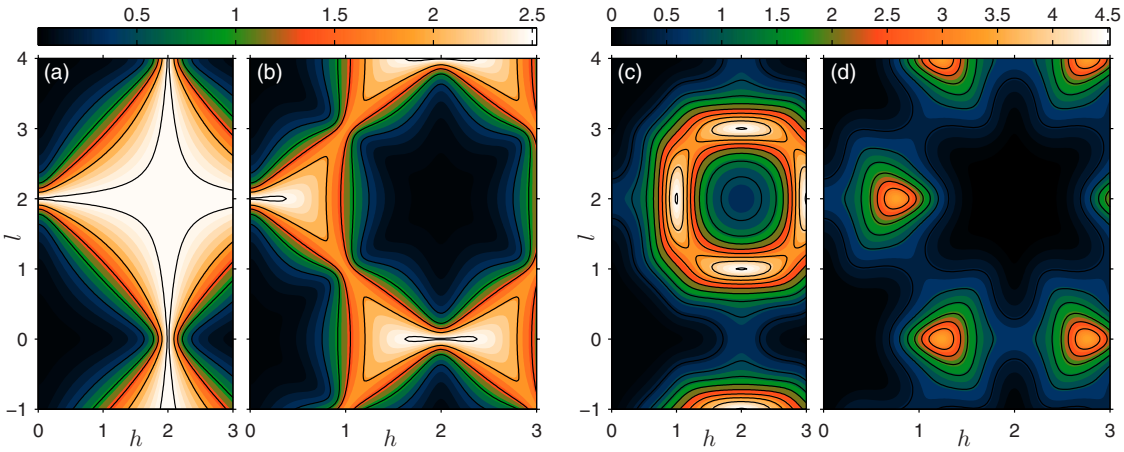

FIG. 3. (Color online) Structure factor $S(\mathbf{q})$ at $T=0.1J_1$. (a) and (b) NN interactions only; (c) and (d) $J_3=0.025J_1$. (a) and (c) $(h0l)$ plane; (b) and (d) (hhl) plane. Contour lines are at the levels marked on the color scale. Compared to a nearest-neighbor model, the effect of AFM J_3 is, first, to suppress and broaden the pinch points, and second, to shift spectral weight so that behavior resembles more the hexagonal cluster scattering. MC simulations yield plots that are indistinguishable by eye.

which they may become less visible. (i) Further neighbor interactions or finite temperature endow the pinch points with a width set by the inverse of the longitudinal correlation length. (ii) The absolute amplitude of the pinch points is set by the inverse of the flux-field stiffness. (iii) The visibility of the pinch points depends also on the relative weight at the pinch points compared to that at the maximum in scattering. We address these mechanisms quantitatively below. (i) For AFM J_3, the longitudinal correlation length is $a\sqrt{\beta(J_1-8J_3)/\lambda}$. The lower bound on λ puts an upper bound on the correlation length of $a\sqrt{(J_1/16J_3-1/2)}$. Even with $J_3 \simeq J_1/150$, the correlation length never exceeds three site spacings and the pinch points are thus never sharp. For FM J_2, a similar argument gives an upper bound on the correlation length of approximately $a\sqrt{(2+J_1/|J_2|)/8.6}$. The effect on the correlation length is shown in Fig. 4(a) for $J_2=-0.025J_1$. (ii) Since the absolute amplitude of the pinch points is set by $1/\lambda$, the lower bound on λ puts an upper bound on the absolute intensity of pinch-point correlations. For AFM J_3, recall that $\lambda > 16\beta J_3$, whereas for FM J_2, we have $\lambda > 8.6\beta J_2$, for $|J_2| \ll J_1$. The pinch-point intensity is shown in Fig. 4(b) for $J_2=-0.025J_1$. (iii) Moreover, as spectral weight shifts away from the pinch points to other wave vectors, the relative amplitude given by the ratio of pinch-point correlations to the maximum in the correlation function decreases even more rapidly. These three mechanisms indicate how pinch points may both be suppressed in amplitude and broadened in width by further neighbor interactions.

2. Hexagonal clusterlike correlations

We have seen how further neighbor terms suppress spectral weight at the pinch points. We turn now to why antiferromagnetically correlated loops of spins such as hexagonal clusters may appear in a model with further neighbor terms. The mechanism is straightforward to explain in the long-wavelength description. For simplicity, we consider first the limit $\beta J_1 \to \infty$ (at finite βJ_2). In this case, pinch points remain infinitely sharp since the local constraint of zero divergence is enforced rigorously, but their amplitude is still suppressed since the flow of the stiffness with temperature is unaffected. The further neighbor terms couple to transverse gradients of the flux fields and the effect of AFM J_3 or FM J_2 is to promote transverse gradients in the flux field. In the continuum picture, maximizing transverse gradients requires having as many small loops of flux as possible; when understood in terms of the lattice geometry, the smallest loops of flux available are the hexagonal clusters. Considered microscopically, it is also clear from Fig. 1 that an AFM J_{3b} is likely to induce antiferromagnetically correlated hexagons of spins.

Following Ref. 5, we define H_0 as the temperature-dependent position of the maximum in scattering along the

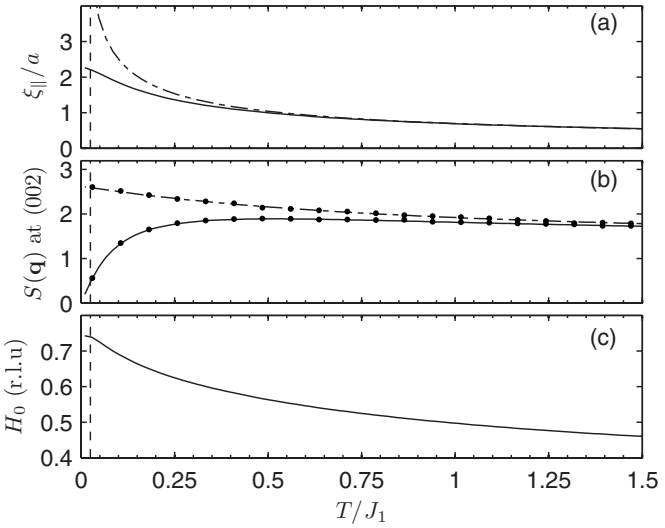

FIG. 4. Temperature dependence of quantities characterizing the scattering, for $J_2=-0.025J_1$. (a) Coulomb-phase correlation length ξ in units of site spacing for NN model (broken line) and for model with nonzero J_2 (solid line). (b) Amplitude of correlation function at pinch point, for both models. (c) Position H_0 of maximum in scattering, as described in text. Dashed line indicates temperature $T=J_2$: the effect of nonzero J_2 extends to $T \gg J_2$. Curves are from SCGA. Points are from simulations on 2048 spins.

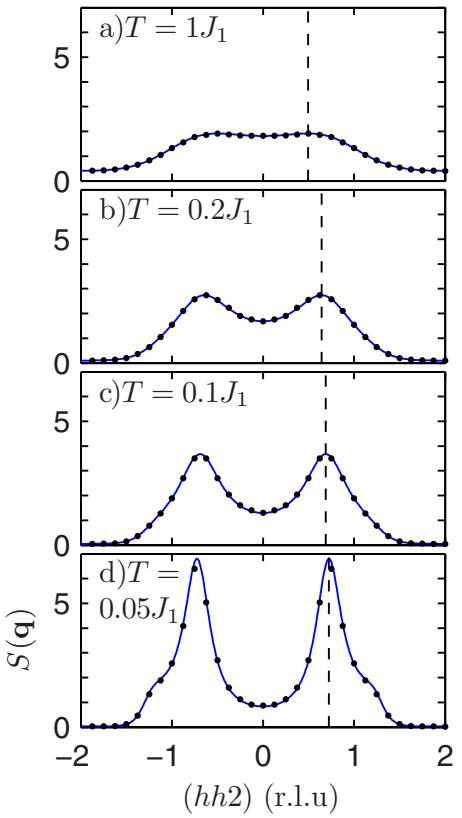

FIG. 5. (Color online) Structure factor along $(hh2)$ for $J_2=-0.025J_1$. Lines are from SCGA, points from simulations on 16 384 spins. The position H_0 at each temperature is indicated by dashed line.

$(hh2)$ direction (see dashed lines in Fig. 5). For FM J_2, at $T=0$, H_0 coincides with h^* given by Chern *et al.*[19] in their Eq. (4), the position of the minimum eigenvalue of the exchange matrix. The evolution of H_0 with temperature extracted from the SCGA is shown in Fig. 4(c). Qualitatively similar behavior for H_0 is found experimentally in $CdFe_2O_4$ (see Fig. 4 in Ref. 5). In contrast, in the NN model (at least classically) the scattering maxima are always found at the pinch points, i.e., $H_0=0$, so the NN model does not provide an explanation for why the maximum in scattering is elsewhere.

In Fig. 6, we show the structure factor on the same planes of reciprocal space as in Fig. 3, but for the case of a FM J_2 rather than an AFM J_3. The qualitative effect is similar, but the characteristic scattering shapes look less like the hexagonal form factor used to explain the scattering in many chromites.

B. Ordering transitions

For $J_3 \ll J_1$, we observe a first-order phase transition at $T_c \simeq 2.2J_3$ in our MC simulations (e.g., see upper inset in Fig. 2). We have not attempted to characterize the ordered state since our focus is on the strongly correlated paramagnet in the window $T_c < T < J_1$. A phase transition is neither predicted by mean-field calculations[17] nor within the theory of

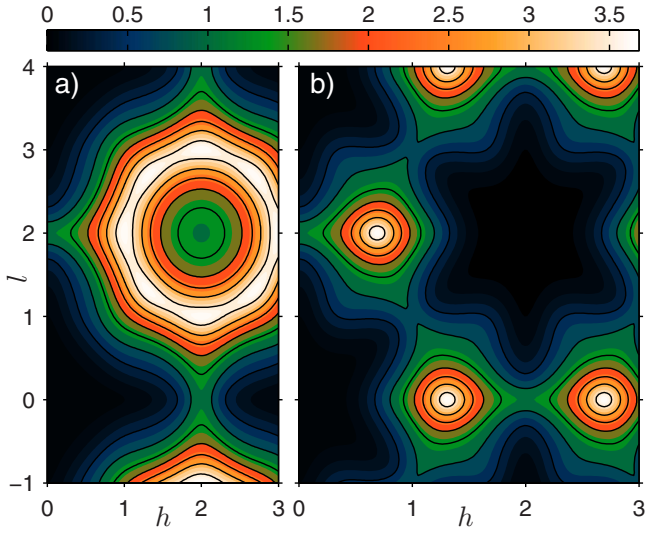

FIG. 6. (Color online) Structure factor at $T=0.1J_1$ with $J_2=-0.025J_1$. Panels as in Fig. 3.

Sec. II A since the interaction minima has a one-dimensional degeneracy in reciprocal space.

In the phase diagram presented by Chern *et al.*,[19] ferromagnetic J_2 leads to incommensurate order at low temperatures consistent with mean-field calculations,[17] but also an intermediate collinear regime, stabilized by thermal fluctuations, with first-order transitions out of the paramagnetic phase. The transition temperature is approximately at $T_c \simeq J_2$, but see Ref. 19 for details.

IV. CONSEQUENCES OF AFM J_2 OR FM J_3

Although the main focus of this paper is further neighbor terms with their sign chosen to suppress pinch-point scattering, we now also consider further neighbor terms with the opposite sign. These enhance pinch-point scattering.

A. Paramagnetic phase

It is clear from Eq. (6) that in the flux description an antiferromagnetic J_2 or FM J_3 penalizes transverse gradients of the flux fields. Qualitatively then, one expects spectral weight to accumulate at small q as short-wavelength fluctuations are suppressed, developing into Bragg peaks as the transverse-flux correlation length diverges at a phase transition.

As seen from the numerical solution of Eq. (3) shown in Fig. 2, FM J_3 causes the stiffness λ to decrease with cooling, and the same behavior is found with AFM J_2. The strength of flux fluctuations is given by the inverse stiffness as in Eq. (7) and consequently this increases. In Fig. 7 we show spin correlations in the paramagnetic phase at the same value of βJ_1 as in Fig. 6: with antiferromagnetic J_2, pinch points are intensified and sharper than for the nearest-neighbor model as expected. Youngblood and Axe[26] considered the Maxwell action with terms penalizing transverse-flux gradients and obtained a similar effect.

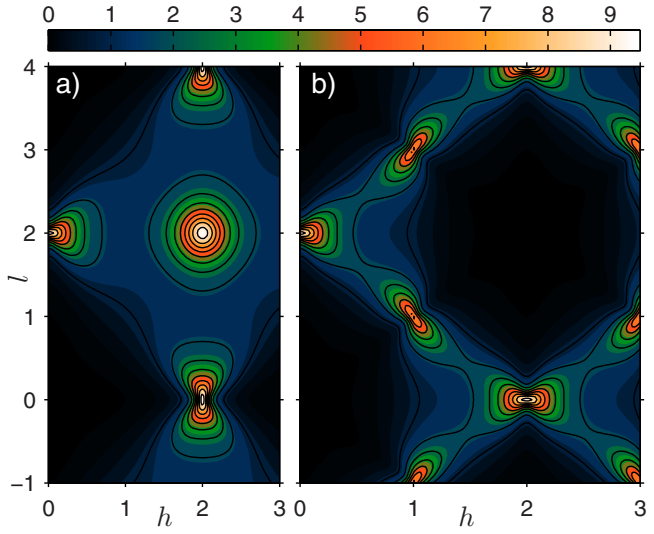

FIG. 7. (Color online) Structure factor $S(\mathbf{q})$ at $T=0.1J_1$ and $J_2=0.025J_1$ in (a) the $(h0l)$ plane and (b) the (hhl) plane. Contour lines are at the levels given in the color scale. Positive J_2 increases pinch-point scattering, and eventually leads to Néel order. The shapes around the pinch points are almost identical to those discussed by Youngblood and Axe (Ref. 26).

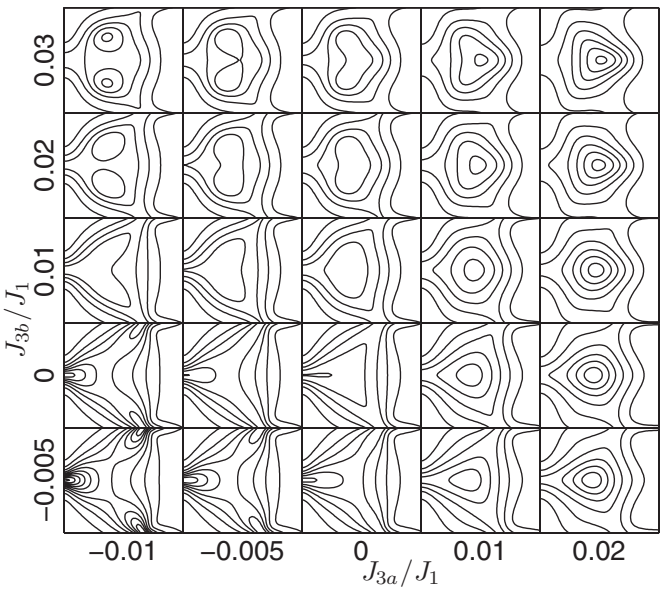

FIG. 8. $S(\mathbf{q})$ in the (hhl) plane for $h\in[0,3/2]$, $l\in[1,3]$ at $T=0.1J_1$, $J_2=0$ and with J_{3a}, J_{3b} interactions treated independently, showing the variety of short-range correlations, and the effects on the pinch point at (002).

B. Ordering transitions

With an AFM $J_2 \ll J_1$, the full model, Eq. (1), has a first-order transition to a $\mathbf{q}=0$ Néel-ordered phase at $T\simeq 3.2J_2$.[19] Within the framework of Sec. II A, the transition is second order and occurs at a lower temperature ($T_c\simeq 2.44J_2$ for $J_1/J_2=100$): the one at which the minimum eigenvalue of the quadratic form in Eq. (2) vanishes. For FM $J_3 \ll J_1$, our simulations reveal a first-order transition at $T\simeq 8|J_3|$ (see lower inset of Fig. 2). In both cases, the transition is to a fully flux-polarized state. Similar transitions occur in other Coulomb-phase systems: for pyrochlore Heisenberg spins, this is $\mathbf{q}=0$ Néel order, for interacting dimer models, a transition to a uniform tilted phase, and in the context of polarization fluctuations in paraelectrics,[26] a ferroelectric transition out of the paraelectric phase.

The transverse-flux correlation length $\xi_\perp$, which is zero for a pure nearest-neighbor model, diverges as $\lambda\to 0$. Flux fluctuations are correlated over larger regions and the divergence of $\xi_\perp$ marks the transition into an ordered phase.

V. GENERAL COMBINATIONS OF FURTHER NEIGHBOR INTERACTION

In Secs. III and IV we took both third-neighbor couplings as equal, but, in general, they need not be and here we consider J_{3a} and J_{3b} as distinct. Within the long-wavelength description, nothing qualitatively changes since further neighbor terms can only act to add gradient terms while renormalizing the stiffness. However, the detailed nature of the short-range paramagnetic correlations is not generic and depends sensitively on the ratios of the different further neighbor couplings. Since this balancing act is separate for each candidate material which our ideas hope to describe, we provide a survey for several different combinations. In Fig. 8, we have plotted paramagnetic correlations in the reciprocal space patch described in the caption for a variety of different J_{3a} and J_{3b} at $T=0.1J_1$. By the arguments of Ref. 19, J_2 acts as $-J_{3a}$ for large enough J_1, so the horizontal axis can be considered approximately to probe $J_{3a}-J_2$.

VI. DYNAMICS AND INELASTIC SCATTERING

We have so far considered only equal time correlations but further neighbor (FN) terms will also affect dynamics. There is an intrinsic precessional dynamics associated with the Heisenberg spins in Eq. (1). Nevertheless, we have shown elsewhere[27] for the NN model that the low-temperature dynamics is dominated by relaxational modes and is very well captured by a purely relaxational stochastic model based on the SCGA of Sec. II A. We find this statement about the low-temperature paramagnet remains true even with FN terms. As evidence for this, we present in Fig. 9 the results of molecular-dynamics simulations using the same methods as in Ref. 27 for the dynamic structure factor, plotted at three different frequencies ω. On the same plot, we show the prediction obtained from including FN terms in the stochastic model. Compared to the static result, the pinch-point scattering at (002) is more suppressed at small ω, and conversely, less suppressed at higher ω. The implications for quasielastic scattering experiments at $\omega\simeq 0$ are that we expect the effects of FN terms to be more conspicuous (and conversely at larger ω, to become less conspicuous) when compared to the static (ω-integrated) scattering which is the main focus of this paper.

The enhanced suppression can be understood by considering the stochastic model in Ref. 27. Within that model the dynamic structure factor is understood as the sum of contributions from the four bands of the interaction matrix, given by

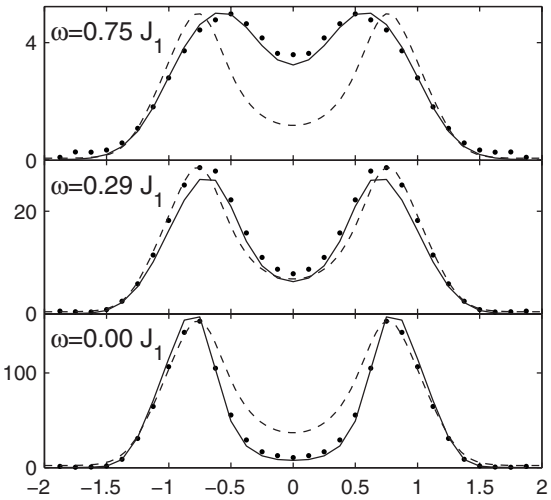

FIG. 9. Points: $S(\mathbf{q},\omega)$ along $(hh2)$ at $T=0.1J_1$, $J_3=0.025J_1$ from simulations. Solid line: $S(\mathbf{q},\omega)$ from stochastic model of Ref. 27 with further neighbor terms. Broken line: $S(\mathbf{q})$ rescaled for comparison. Pinch points are more suppressed at small ω and conversely less suppressed at high ω.

$$S(\mathbf{q},\omega)=\sum_{\mu=1}^{4} g_\mu(\mathbf{q}) f_\mu(\mathbf{q},\omega), \tag{11}$$

where the $g_\mu(\mathbf{q})$ are form factors, independent of temperature, and where the thermal weight and dynamics for each band are contained in the functions $f_\mu(\mathbf{q},\omega)$. The quadratic form in Eq. (2) has eigenvalues $\alpha_\mu(\mathbf{q})$, labeled by band index μ, which determine relaxation rates $\Gamma_\mu(\mathbf{q})\propto\alpha_\mu(\mathbf{q})$ and these enter the dynamic structure factor through the relation

$$f_\mu(\mathbf{q},\omega)=\alpha_\mu^{-1}(\mathbf{q})\frac{2\Gamma_\mu(\mathbf{q})}{\omega^2+\Gamma_\mu(\mathbf{q})^2}. \tag{12}$$

By integrating over ω we obtain the static structure factor, which has the form of Eq. (11), but with $\alpha_\mu^{-1}(\mathbf{q})$ in place of $f_\mu(\mathbf{q},\omega)$.

With only nearest-neighbor interactions, the two lowest bands (which are dominant at low temperature) are dispersionless and degenerate, which has two consequences: the $\mathbf{q}$ dependence arises entirely from the form factors in Eq. (11) since the relevant f_μ are independent of $\mathbf{q}$, and the ω dependence approximately factorizes out. With FN interactions, the lowest bands acquire dispersion and the relevant f_μ are no longer independent of $\mathbf{q}$. If their ratio in the static case for band μ at $\mathbf{q}_1$ and $\mathbf{q}_2$ is r, then in the dynamic case with $\omega=0$ it is r^2. This is why the suppression effects we have discussed in this paper, which correspond to $r\neq 1$, are enhanced in quasielastic scattering. Further discussion of dynamical correlations is given in Ref. 21.

VII. ESTIMATES OF FURTHER NEIGHBOR EXCHANGE

Evidence from *ab initio* calculations suggests third-neighbor couplings are important in a number of relevant compounds. In a study of ACr_2X_4 spinels including zinc and cadmium chromite, Yaresko [28] finds that AFM coupling between third neighbors is important in all the compounds considered, and that the ratio $J_{3b}/J_{3a}\simeq 0.5$ for Zn and Cd. (Our J_{3a} and J_{3b} are labeled as $J_{3'}$ and $J_{3''}$ in Ref. 28). A separate *ab initio* study of $CdCr_2O_4$ finds $J_3/J_1\simeq 0.3$ where both third-neighbor couplings are taken with the same strength.[24] In both $ZnFe_2O_4$ and $CdFe_2O_4$, Cheng[29] also reports that third-neighbor interactions are estimated to be much stronger than second-neighbor interactions and on the same order in magnitude as first-neighbor interactions. This result is in broad agreement with a study of third-neighbor interactions in $ZnFe_2O_4$ (Ref. 20).

Experimental estimates of nearest-neighbor and next-nearest-neighbor exchange from susceptibility measurements[30] find for $CdCr_2O_4$ a FM $J_2\simeq -0.3J_1$ but for $ZnCr_2O_4$ an AFM $J_2\simeq 0.15J_1$. From our results in Sec. IV, the latter would imply scattering quite different from that observed; we have not examined the reliability of the model used in Ref. 30 in the presence of third-neighbor terms, but believe that $ZnCr_2O_4$ is unlikely to be described by a Heisenberg model with AFM J_2 without other further neighbor terms included.

VIII. DISCUSSION

The appearance of antiferromagnetically correlated hexagonal clusters in the spinels is certainly puzzling in the context of a pure nearest-neighbor model, since properties of the NN model have been reliably calculated and give different behavior. In Sec. VII, we discussed evidence for further neighbor exchange and found that AFM third-neighbor exchange is important in many of the compounds we have been discussing. We should also address other possibilities.

It has been suggested that spin clusters are induced by magnetoelastic coupling.[3] However, we note that among the compounds where spin clusters have been reported, $CdCr_2O_4$ undergoes a c-axis elongation,[4] whereas both $ZnCr_2O_4$ and $MgCr_2O_4$ undergo a c-axis contraction and $CdFe_2O_4$ has no structural transition at all; it is not clear how magnetoelastic coupling which leads to different structural transitions should explain the clusterlike scattering common to all of these materials. Moreover, scattering in $Y(Sc)Mn_2$ is broadly similar to the spinels,[6] but we expect the nature of spin-lattice coupling to be different, and this throws further doubt over the idea that magnetoelastic coupling may be universally responsible for clusterlike scattering.

We should also discuss the temperature dependence of our results. The images in Figs. 3 and 6 are for a single temperature, where the hexagonal clusterlike scattering is most visible; at lower temperatures, however, the further neighbor terms induce magnetic phase transitions as discussed in the text. If indeed further neighbor terms are required to explain the hexagonal cluster scattering, we may also expect to observe the associated magnetic phase transitions. In the chromites, we can avoid the issue by assuming the magnetic phase transition is pre-empted by the structural transitions driven by the independent mechanism of spin-lattice coupling; this is not entirely satisfactory as an explanation, since $CdFe_2O_4$ shows neither a structural transition nor development of any Bragg peaks at any temperature. It is possible

that quantum fluctuations or disorder can stabilize the paramagnetic phase,[31] but it is hard to be conclusive about a range of materials at once, and the role of further neighbor exchange should be assessed individually for different materials.

We have presented further neighbor exchange as the simplest extra interaction which gives hexagonal cluster scattering, but further neighbor exchange is not the only perturbation one could imagine. Others include Dzyaloshinsky-Moriya interactions[32,33] and biquadratic exchange, which can appear microscopically or as an effective term taking into account quantum fluctuations.[34] In future work it would be interesting to consider the effects of these other perturbations on the paramagnetic phase. The present results are sufficient to show that further neighbor exchange of a realistic strength can dramatically alter the diffuse scattering and should not be ignored in comparing experimental results to simple theoretical models.

Clusters should be understood, then, as short-range order in a strongly correlated state. A similar view is expressed by Yavors'kii *et al.*[7] when considering clusterlike scattering in spin ices; their analysis including further neighbor terms suggests that clusterlike scattering is the property of a strongly correlated liquid state which is sensitive to weak perturbations rather than due to the emergence of "real" clusters.

Our results potentially explain why a clear signature of algebraic correlations is missing in candidates for pyrochlore Heisenberg magnets. Small further neighbor interactions are sufficient to wash out the pinch points. Our results may have implications for other pyrochlore models, but in Ising models where the ice rules are exponentially enforced, we do not expect the dramatic broadening we observe in the Heisenberg model. Nevertheless, the suppression of pinch-point scattering amplitude is expected, and we note that in Ref. 8 such a suppression is reported in the spin ice $Ho_2Ti_2O_7$.

In summary, we have studied the effect of further neighbor interactions on the low-temperature paramagnetic phase of the frustrated Heisenberg antiferromagnet on the pyrochlore lattice. Further neighbor terms induce transitions to ordered phases, but they also have a striking effect on paramagnetic correlations. In the description of the low-temperature paramagnet as a Coulomb phase, further neighbor terms cause the Coulomb-phase coupling constant, or stiffness, to flow. Pinch points in diffuse scattering have their amplitude and width controlled by the stiffness, and even very weak further neighbor terms can cause pinch points to be suppressed in amplitude and broadened. With FM J_2 or AFM J_3, paramagnetic scattering is altered to resemble more the hexagonal cluster scattering that is often observed in experimental systems, notably spinels. Further neighbor terms then provide a mechanism for the previously unexplained clusterlike scattering in frustrated spinels.

ACKNOWLEDGMENTS

P.C. acknowledges helpful discussions with M. Gingras and S. Bramwell. This work was supported in part by EPSRC under Grant No. EP/D050952/1.

APPENDIX A: LATTICE DEFINITIONS

We take throughout a conventional cubic unit cell of side 1 and use a to refer to the pyrochlore nearest-neighbor distance, so that $a^2=1/8$. The midpoints of the tetrahedra form a diamond lattice with site spacing $\sqrt{3/16}$.

The pyrochlore lattice is a face-centered-cubic (fcc) lattice decorated with a tetrahedron at each fcc site. Using the following choice of fcc basis vectors:

$$\mathbf{a}_1=\frac{1}{2}(\mathbf{e}_y+\mathbf{e}_z),\quad \mathbf{a}_2=\frac{1}{2}(\mathbf{e}_z+\mathbf{e}_x),\quad \mathbf{a}_3=\frac{1}{2}(\mathbf{e}_x+\mathbf{e}_y), \tag{A1}$$

then (up to an arbitrary displacement) the corners of the tetrahedra appear at positions

$$\mathbf{c}_\mu \in \left\{0,\frac{\mathbf{a}_1}{2},\frac{\mathbf{a}_2}{2},\frac{\mathbf{a}_3}{2}\right\}, \tag{A2}$$

where μ labels the four sublattices and runs from 1–4, as in Fig. 1. The Fourier transforms we use are

$$S_\mu(\mathbf{r})=\frac{1}{\sqrt{N}}\sum_{\mathbf{q}\in \mathrm{BZ}} S_\mu(\mathbf{q})e^{i\mathbf{q}\cdot(\mathbf{r}+\mathbf{c}_\mu)},$$

$$S_\mu(\mathbf{q})=\frac{1}{\sqrt{N}}\sum_{\mathbf{r}} S_\mu(\mathbf{r})e^{-i\mathbf{q}\cdot(\mathbf{r}+\mathbf{c}_\mu)}, \tag{A3}$$

where $\mathbf{r}$ runs over N fcc lattice sites so that there are $4N$ spins in total.

APPENDIX B: INTERACTION MATRICES

As described in the main text, with $A_{ij}^{(n)}$ denoting the adjacency matrix that is 1 if sites i and j are nth neighbors and zero otherwise, the interaction matrices are chosen to be $V_{ij}^{(1)}=A_{ij}^{(1)}+2\delta_{ij}$; $V_{ij}^{(2)}=A_{ij}^{(2)}+4\delta_{ij}$; $V_{ij}^{(3a)}=A_{ij}^{(3a)}-6\delta_{ij}$; and $V_{ij}^{(3b)}=A_{ij}^{(3b)}-6\delta_{ij}$. This choice of diagonal entries is made so that when expressed in reciprocal space according to Eq. (A3) and using the basis change in Eq. (5), the 3×3 subblock which acts among the flux components vanishes at $\mathbf{q}=0$. This ensures that λ can be interpreted as the stiffness of the flux fluctuations.

The matrix elements for the interactions can be found in Ref. 17, although in a different basis so we provide them here using our conventions. We first define the fcc displacement vectors $\mathbf{t}_{\mu\nu}=2(\mathbf{c}_\mu-\mathbf{c}_\nu)$, where the $\mathbf{c}_\mu$ are as in Appendix A. After Fourier transform the matrix elements of the adjacency matrices are given by

$$A^{(1)}(\mathbf{q})_{12}=2\cos\left(\frac{\mathbf{q}\cdot\mathbf{t}_{12}}{2}\right)$$

and

$$A^{(2)}(\mathbf{q})_{12} = 2\cos\left(\frac{\mathbf{q}\cdot(\mathbf{t}_{13}+\mathbf{t}_{23})}{2}\right) + 2\cos\left(\frac{\mathbf{q}\cdot(\mathbf{t}_{14}+\mathbf{t}_{24})}{2}\right)$$

with diagonal elements zero and the rest by permutation.

Furthermore, third-neighbor couplings are diagonal giving

$$A^{(3a)}(\mathbf{q})_{11} = 2\cos(\mathbf{q}\cdot\mathbf{t}_{12}) + 2\cos(\mathbf{q}\cdot\mathbf{t}_{13}) + 2\cos(\mathbf{q}\cdot\mathbf{t}_{14})$$

and

$$A^{(3b)}(\mathbf{q})_{11} = 2\cos(\mathbf{q}\cdot\mathbf{t}_{23}) + 2\cos(\mathbf{q}\cdot\mathbf{t}_{24}) + 2\cos(\mathbf{q}\cdot\mathbf{t}_{34}).$$

To derive the long-wavelength theory in the flux sector, we implement a change in basis as described in the main text using the orthogonal matrix

$$P = \frac{1}{2}\begin{pmatrix} 1 & 1 & 1 & 1 \\ 1 & 1 & -1 & -1 \\ 1 & -1 & 1 & -1 \\ 1 & -1 & -1 & 1 \end{pmatrix}$$

and then take the small-$\mathbf{q}$ limit. This procedure gives the following interactions:

$$PV^{(1)}P^{\mathrm{T}} \simeq \begin{pmatrix} 8-a^2q^2 & -a^2q_yq_z & -a^2q_xq_z & -a^2q_xq_y \\ -a^2q_yq_z & a^2q_x^2 & a^2q_xq_y & a^2q_xq_z \\ -a^2q_xq_z & a^2q_xq_y & a^2q_y^2 & a^2q_yq_z \\ -a^2q_xq_y & a^2q_xq_z & a^2q_yq_z & a^2q_z^2 \end{pmatrix}$$

and

$$PV^{(2)}P^{\mathrm{T}} \simeq \begin{pmatrix} 16-6a^2q^2 & 2a^2q_yq_z & 2a^2q_xq_z & 2a^2q_xq_y \\ 2a^2q_yq_z & -2a^2q_x^2 & -2a^2q_xq_y & -2a^2q_xq_z \\ 2a^2q_xq_z & -2a^2q_xq_y & -2a^2q_y^2 & -2a^2q_yq_z \\ 2a^2q_xq_y & -2a^2q_xq_z & -2a^2q_yq_z & -2a^2q_z^2 \end{pmatrix} + 4a^2\begin{pmatrix} 0 & 0 & 0 & 0 \\ 0 & q_y^2+q_z^2 & 0 & 0 \\ 0 & 0 & q_x^2+q_z^2 & 0 \\ 0 & 0 & 0 & q_x^2+q_y^2 \end{pmatrix}$$

and

$$PV^{(3a)}P^{\mathrm{T}} \simeq 4a^2\begin{pmatrix} -q^2 & -q_yq_z & -q_xq_z & -q_xq_y \\ -q_yq_z & -q_x^2 & -q_xq_y & -q_xq_z \\ -q_xq_z & -q_xq_y & -q_y^2 & -q_yq_z \\ -q_xq_y & -q_xq_z & -q_yq_z & -q_z^2 \end{pmatrix} - 4a^2\begin{pmatrix} 0 & 0 & 0 & 0 \\ 0 & q_y^2+q_z^2 & 0 & 0 \\ 0 & 0 & q_x^2+q_z^2 & 0 \\ 0 & 0 & 0 & q_x^2+q_y^2 \end{pmatrix},$$

$$PV^{(3b)}P^{\mathrm{T}} \simeq 4a^2\begin{pmatrix} -q^2 & q_yq_z & q_xq_z & q_xq_y \\ q_yq_z & q_x^2 & q_xq_y & q_xq_z \\ q_xq_z & q_xq_y & q_y^2 & q_yq_z \\ q_xq_y & q_xq_z & q_yq_z & q_z^2 \end{pmatrix} - 4a^2\begin{pmatrix} 0 & 0 & 0 & 0 \\ 0 & 2q_x^2+q_y^2+q_z^2 & 0 & 0 \\ 0 & 0 & q_x^2+2q_y^2+q_z^2 & 0 \\ 0 & 0 & 0 & q_x^2+q_y^2+2q_z^2 \end{pmatrix}.$$

In each case we have split the interaction into a part which acts like J_1 within the flux-field subspace and another part. Chern *et al.*[19] argued that J_2 and $-J_{3a}$ have the same effect if $J_1 \to \infty$. This fact is evident in the small-q expansions above. If the two symmetry inequivalent third-neighbor couplings are taken to have the same strength, as done by Reimers *et al.*,[17] then the rotated third-neighbor interaction matrix is particularly simple

$$P[V^{(3a)} + V^{(3b)}]P^{\mathrm{T}} \simeq -8a^2\mathrm{diag}(q^2). \tag{B1}$$

Integrating out $M(\mathbf{q})$ in the long-wavelength limit leads to couplings at $\mathcal{O}(q^4)$ between the components $B_i(\mathbf{q})$, which we have ignored in the analysis at small $\mathbf{q}$ in Sec. II B.

APPENDIX C: LOCATIONS OF PINCH POINTS IN STRUCTURE FACTOR

The experimental probe in scattering experiments is the structure factor $S(\mathbf{q})=4\langle|M(\mathbf{q})|^2\rangle$. However the long-wavelength physics is in the field $\mathbf{B}$ near $\mathbf{q}=0$. In this appendix we determine the places in reciprocal space where signatures of the behavior of $\mathbf{B}$ are visible.

For $\mathbf{K}$ a reciprocal lattice vector we have

$$S_\mu(\mathbf{q}+\mathbf{K}) = e^{i\mathbf{K}\cdot\mathbf{c}_\mu}S_\mu(\mathbf{q}). \tag{C1}$$

Taking $\mathbf{b}_i$ as the reciprocal basis to $\mathbf{a}_j$, then a reciprocal lattice vector $\mathbf{K}=n_1\mathbf{b}_1+n_2\mathbf{b}_1+n_3\mathbf{b}_1$ is

$$\mathbf{K} = 2\pi[(n_2 + n_3 - n_1)\hat{\mathbf{x}} + (n_3 + n_1 - n_2)\hat{\mathbf{y}} + (n_1 + n_2 - n_3)\hat{\mathbf{z}}]. \tag{C2}$$

Bearing in mind the definitions of $\mathbf{c}_\mu$, the phase factors for the different sublattices are 1, $(-1)^{n_1}$, $(-1)^{n_2}$, $(-1)^{n_3}$. It follows that:

$$M(\mathbf{q} + \mathbf{K}) = \frac{1}{4}[v_0 M(\mathbf{q}) + \mathbf{v} \cdot \mathbf{B}(\mathbf{q})], \tag{C3}$$

where

$$v_0 = 1 + (-1)^{n_1} + (-1)^{n_2} + (-1)^{n_3} \tag{C4}$$

and

$$\mathbf{v} = \begin{pmatrix} 1 + (-1)^{n_1} - (-1)^{n_2} - (-1)^{n_3} \\ 1 - (-1)^{n_1} + (-1)^{n_2} - (-1)^{n_3} \\ 1 - (-1)^{n_1} - (-1)^{n_2} + (-1)^{n_3} \end{pmatrix}. \tag{C5}$$

If all n_i are even, the structure factor in the vicinity of the reciprocal lattice point probes only the total magnetization. If only one n_i is even, it probes $\mathbf{v} \cdot \mathbf{B}$ and in the two other cases, there are contributions from both $M(\mathbf{q})$ and $\mathbf{v} \cdot \mathbf{B}(\mathbf{q})$.

APPENDIX D: OTHER RESULTS

We also provide here the structure factor for the nearest-neighbor model. In the notation of Isakov *et al.*,[14] where $c_{ab} = \cos(\frac{q_a + q_b}{4})$ and $c_{\overline{ab}} = \cos(\frac{q_a - q_b}{4})$ with $Q = c_{xy}^2 + c_{\overline{xy}}^2 + c_{yz}^2 + c_{\overline{yz}}^2 + c_{xz}^2 + c_{\overline{xz}}^2 - 3$ and further defining $s_a^2 \equiv \sin^2(\frac{q_a}{4})$ and $c_{(ab)} \equiv c_{ab} + c_{\overline{ab}}$, the static structure factor is

$$S(\mathbf{q})_{\mathrm{NN}} = \frac{1}{\lambda}\left[2 + \frac{(2 - c_{(xy)} - c_{(yz)} - c_{(zy)})t\lambda + \frac{1}{2}(t\lambda)^2 - 4[c_{(xy)}s_z^2 + c_{(yz)}s_x^2 + c_{(zx)}s_y^2]}{3 - Q + 2t\lambda + \frac{1}{4}(t\lambda)^2}\right], \tag{D1}$$

where $t = T/J_1$ and λ is the solution of Eq. (3). At $T \ll J_1$, the zero-temperature solution $\lambda = 3/2$ is a good approximation (see Fig. 2). Up to an overall rescaling due to the choice of spin length, Eq. (D1) reduces in the limit $t \to 0$ to the zero-temperature form provided by Isakov *et al.*[14]

*conlon@thphys.ox.ac.uk

[1] For introduction see R. Moessner, Can. J. Phys. **79**, 1283 (2001); J. T. Chalker, in *Highly Frustrated Magnetism*, edited by C. Lacroix, P. Mendels, and F. Mila (Springer, Berlin, 2010).
[2] S. Lee, C. Broholm, W. Ratcliff, G. Gasparovic, Q. Huang, T. Kim, and S. Cheong, Nature (London) **418**, 856 (2002).
[3] K. Tomiyasu, H. Suzuki, M. Toki, S. Itoh, M. Matsuura, N. Aso, and K. Yamada, Phys. Rev. Lett. **101**, 177401 (2008).
[4] J.-H. Chung, M. Matsuda, S.-H. Lee, K. Kakurai, H. Ueda, T. J. Sato, H. Takagi, K.-P. Hong, and S. Park, Phys. Rev. Lett. **95**, 247204 (2005).
[5] K. Kamazawa, S. Park, S.-H. Lee, T. J. Sato, and Y. Tsunoda, Phys. Rev. B **70**, 024418 (2004).
[6] R. Ballou, E. Lelièvre-Berna, and B. Fåk, Phys. Rev. Lett. **76**, 2125 (1996).
[7] T. Yavors'kii, T. Fennell, M. J. P. Gingras, and S. T. Bramwell, Phys. Rev. Lett. **101**, 037204 (2008).
[8] T. Fennell, P. P. Deen, A. R. Wildes, K. Schmalzl, D. Prabhakaran, A. T. Boothroyd, R. J. Aldus, D. F. McMorrow, and S. T. Bramwell, Science **326**, 415 (2009).
[9] S.-H. Lee *et al.*, J. Phys. Soc. Jpn. **79**, 011004 (2010).
[10] J. N. Reimers, Phys. Rev. B **45**, 7287 (1992).
[11] R. Moessner and J. T. Chalker, Phys. Rev. Lett. **80**, 2929 (1998).
[12] R. Moessner and J. T. Chalker, Phys. Rev. B **58**, 12049 (1998).
[13] M. P. Zinkin, M. J. Harris, and T. Zeiske, Phys. Rev. B **56**, 11786 (1997).
[14] S. V. Isakov, K. Gregor, R. Moessner, and S. L. Sondhi, Phys. Rev. Lett. **93**, 167204 (2004).
[15] C. L. Henley, Phys. Rev. B **71**, 014424 (2005).
[16] C. L. Henley, arXiv:0912.4531 (unpublished).
[17] J. N. Reimers, A. J. Berlinsky, and A.-C. Shi, Phys. Rev. B **43**, 865 (1991).
[18] D. Tsuneishi, M. Ioki, and H. Kawamura, J. Phys.: Condens. Matter **19**, 145273 (2007).
[19] G.-W. Chern, R. Moessner, and O. Tchernyshyov, Phys. Rev. B **78**, 144418 (2008).
[20] Y. Yamada, K. Kamazawa, and Y. Tsunoda, Phys. Rev. B **66**, 064401 (2002).
[21] P. H. Conlon, Ph.D. thesis, University of Oxford (2010).
[22] B. Canals and D. A. Garanin, Can. J. Phys. **79**, 1323 (2001).
[23] H. E. Stanley, Phys. Rev. **176**, 718 (1968).
[24] G.-W. Chern, C. J. Fennie, and O. Tchernyshyov, Phys. Rev. B **74**, 060405 (2006).
[25] F. Alet, G. Misguich, V. Pasquier, R. Moessner, and J. L. Jacobsen, Phys. Rev. Lett. **97**, 030403 (2006).
[26] R. W. Youngblood and J. D. Axe, Phys. Rev. B **23**, 232 (1981).
[27] P. H. Conlon and J. T. Chalker, Phys. Rev. Lett. **102**, 237206 (2009).
[28] A. N. Yaresko, Phys. Rev. B **77**, 115106 (2008).
[29] C. Cheng, Phys. Rev. B **78**, 132403 (2008).
[30] C. Kant, J. Deisenhofer, T. Rudolf, F. Mayr, F. Schrettle, A. Loidl, V. Gnezdilov, D. Wulferding, P. Lemmens, and V. Tsurkan, Phys. Rev. B **80**, 214417 (2009).
[31] T. E. Saunders and J. T. Chalker, Phys. Rev. B **77**, 214438 (2008).
[32] V. N. Kotov, M. Elhajal, M. E. Zhitomirsky, and F. Mila, Phys. Rev. B **72**, 014421 (2005).
[33] M. Elhajal, B. Canals, R. Sunyer, and C. Lacroix, Phys. Rev. B **71**, 094420 (2005).
[34] B. E. Larson and C. L. Henley, arXiv:0811.0955 (unpublished).